Mn-Co spinel coatings on Crofer 22 APU by electrophoretic deposition: up scaling, performance in SOFC stack at 850°C and compositional modifications

A.G. Sabato[1], E. Zanchi[2], S. Molin[3], G. Cempura[4], H. Javed[5], K. Herbrig[5], C. Walter[5], A. R. Boccaccini[6], F. Smeacetto[2]*

1. Institut de Recerca en Energia de Catalunya (IREC), Jardins de les Dones de Negre, 1, 2ª pl., 08930 Sant Adrià de Besòs, Barcelona, Spain

2. Department of Applied Science and Technology, Politecnico di Torino, Corso Duca degli Abruzzi 24, 10129 Torino, Italy

3. Faculty of Electronics, Telecommunications and Informatics, Gdańsk University of Technology, ul. G. Narutowicza 11/12, 80-233 Gdańsk, Poland

4. AGH University of Science and Technology, al. Mickiewicza 30, 30-059, Krakow, Poland

5. Sunfire GmbH, Gasanstaltstraße 2, 01237 Dresden, Germany

6. Department of Materials Science and Engineering, University of Erlangen-Nuremberg, Cauerstr. 6, 91058 Erlangen, Germany

*corresponding author: e-mail federico.smeacetto@polito.it

Abstract

Ceramic coatings for metallic interconnects play a key role in limiting corrosion and chromium evaporation in solid oxide cells. This study presents the upscaling of the electrophoretic deposition (EPD) technique to process Mn-Co spinels on real-dimension Crofer 22 APU interconnects and the test in a SOFC stack. Area specific resistance of long term test conducted for 5000 hours at 850°C demonstrated that two-steps sintering has a significant influence on the coating performance; an area specific resistance degradation rate of 0.5 mΩ cm^2 kh^{-1} is recorded. Stack test, operated in fuel cell mode at 850°C for 3000h under application of 227 mA/cm^2, including 5 thermal cycles, demonstrated the effectiveness of the electrophoretically deposited Mn-Co spinel in limiting the oxide scale growth on the Crofer 22 APU. An advanced post mortem investigation showed the effectiveness of the EPD ceramic coating, even when considering different and complex surfaces of the Crofer 22 APU.

Introduction

Chromia-forming ferritic stainless steels (FSSs) are widely used as metallic interconnects (IC) in solid oxide cells stacks because of their coefficient of thermal expansion (CTE) matching the ceramic parts of the stack, good performance, low cost and easier processing in comparison with their ceramic counterparts. The most used FSSs up to now have been Crofer 22 APU, AISI 430 and AISI 441.

The metallic interconnect, during its operation in the oxygen electrode compartment of a solid oxide cells (SOC) stack, reacts with oxygen and steam forming volatile Cr (VI) species that migrate and react at the electrolyte-oxygen electrode three phase boundary, thus "poisoning" the electrochemical activity with detrimental consequences on the stack performance. Chromium poisoning is one of the most important degradation phenomena [1-3].

The application of ceramic protective coatings to the IC has been proved as a practical and effective method to limit volatile Cr(VI) species, and at the same time to reduce the growth rate of underlying poor conductive oxide scale, due to inward diffusion of oxygen from the oxidising atmosphere [4].

Previous research has confirmed the critical role played by ceramic coatings in maintaining a favourable stack performance during operation and how such coatings can lower the oxidation rate and block evaporation of chromium, thus increasing the lifetime of the solid oxide cells stack. In particular, manganese cobaltite spinel-based coatings have attracted great consideration due to their high electrical conductivity at 750-850 °C (up to 60 S cm^{-1}) and a CTE matching with the ferritic stainless steels FSSs [5].

A considerable amount of literature has been published on Mn-Co spinel based coatings [6-10]. Most of the studies in the field of ceramic coatings for metallic IC focus on thin film deposition methods like PVD/sputtering [11], thermal oxidation [12], thermal spray [7,13,14], thermal co-evaporation [15]; even if dense structures can be formed at low temperatures, a limitation of the thickness to only few µm can be detrimental to physically limit Cr diffusion and evaporation from the underlying steel or the oxide scale growth [16]. In addition, these techniques may not lead to uniform deposition in case of IC complex shapes (i.e. channelled surfaces) in comparison with wet methods such as electroplating or electrophoretic deposition [17-19].

Fu et al. [18] have investigated the uniformity of protective layers obtained by magnetron sputtering, reporting a much lower thickness of the deposited coating on the side walls and on the valleys of a channelled IC.

On the other hand, Talic et al. [19] successfully assessed electrophoretic deposition (EPD) as suitable technique to obtain a uniform thickness of the protective layer even on complex shapes. In addition,

their work pointed out that the post-deposition treatments (i.e. sintering) can also have substantial effects related to the interconnect shape. In particular, after the sintering step, cracks have been detected on concave interconnect surfaces, while convex and flat surfaces seem to be less critical.

Many works up to now have focused on the EPD technique to obtain ceramic protective coatings for these applications including: Mn-Co spinels [9,16,19-28], Mn-Cu-based spinels [29-31] or strontium-doped lanthanum manganite (LSM) [32,33]. This is due to the relatively simplicity of the EPD technique, the possibility to obtain thick layers in very short times, the absence (or low presence) of organic binder, the potential to coat very large areas in short time and the suitability to be used in channelled or curved surfaces [34].

Furthermore, the introduction of a sintering step in reducing atmosphere has been demonstrated to enhance the densification of the protective layer [23,35]. Zhang et al. reported a significant improvement in terms of ASR and coating densification of Mn-Co spinel, sintered in H_2/H_2O instead of static air [28].

EPD is suitable to scaling up from laboratory scale to industrial one using inexpensive equipment and minor adjustments in comparison with the laboratory process [36,37]. However, to the authors' best knowledge; there is no evidence of the successful implementation of this EPD to produce effective MnCo-spinel based coatings for SOC applications on real dimension IC plates with subsequent stack assembly and test. Indeed, due to typical dimensions of an IC plate a uniform deposition is required on a very larger area (~ 200 cm^2), in comparison with typical laboratory samples (~ 1 cm^2). A large sample surface may require particular attention or slight modifications of many steps of the whole process, in comparison with the laboratory scale (i.e. stirring and dispersion of the suspension, drying of the coated objects) or it may become necessary to adjust the formulation of the suspension.

Previous studies have explored the interrelation between results from SOFC stacks tested for different times and coated interconnects degradation phenomena [38,39]. In the work by Bianco et al. [39] for example, Mn-Co spinel layer was deposited onto AISI 441 steel by wet powder spraying technique. Menzler et al. [38] analysed the performance and the degradation phenomena of a short stack tested for more than 30,000h, involving Fe-doped Mn-Co spinel coating obtained by plasma spraying.

To the authors' best knowledge, there is a lack of data from real stack tests with IC coated by EPD. The present paper is thus the first study presenting the testing of IC plates coated by EPD in a real stack operated for 3000 hours at 850 °C, together with a detailed post mortem analysis. This work

represents a step forward in the implementation of EPD as sound and practical deposition method of ceramic coatings on industrial scale and lays the groundwork for future consideration and utilization of this low cost and versatile technique in the field of ceramic protective coatings for SOCs.

Experimental

Coatings deposition and sintering

Commercial powder of $Mn_{1.5}Co_{1.5}O_4$ (MCO) from American Elements and with a mean particle size of 0.36 µm was used to prepare the EPD suspension. The recipe of the suspension is reported elsewhere [16]. In order to study the morphology and performance of the obtained coatings, all the depositions were made on real dimension plates with a channelled surface. The plates were 160x180 mm^2 provided by Sunfire GmbH. Five litres of suspension were prepared to coat the real plates. Due to the high concentration of the solid part (37.5 gL^{-1}) and to the limited number of plates to be coated, the depletion of the solid part in the suspension was assumed to be negligible after each deposition. Before the deposition, Teflon tape was used to mask the regions of the plate that necessitated not to be coated (i.e. glass sealing area). The tape was then removed after the deposition and before the sintering process.

The EPD process was a cathodic deposition process with three-electrodes geometry; the deposition occurred on the cathode. The plates to be coated on both sides were placed in between two counter electrodes (stainless steel plates of the same dimension of the IC). The distance between the plate and each counter electrode was fixed at 1 cm. Before each deposition, the suspension was subjected to 3 cycles of dispersion, alternating stirring for 5 min and ultrasonic bath for 5 min. The deposition was performed by controlling the voltage at a fixed value of 50 V for 60 sec. After the deposition the plates were dried in air at room temperature for 10 min while being horizontally aligned. A schematic diagram showing the EPD cathodic deposition method with a three electrodes geometry is shown in Figure 1.

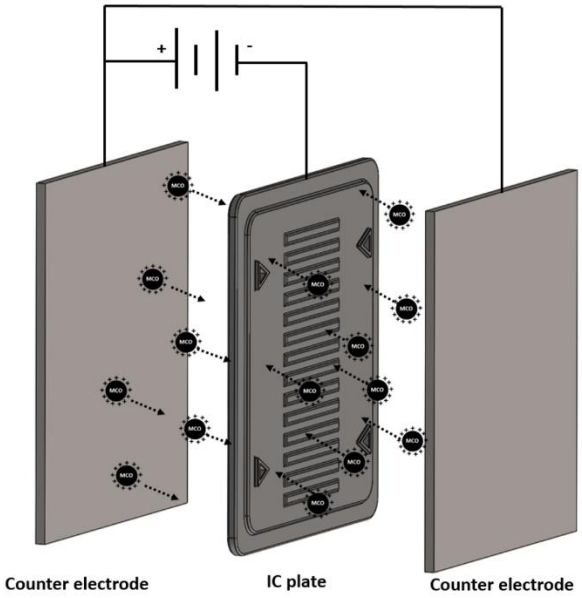

Figure 1. Schematic diagram showing the EPD cathodic deposition method with a three-electrodes geometry.

Two different treatments of sintering were considered:

1) Two-step sintering: the sintering was carried out in two subsequent thermal treatments, both at 900 °C for 2 h (heating rate 10 °C/min). The first one in reducing atm. N_2/H_2 (H_2 1 vol.%) in order to reduce the spinel to MnO and metallic Co, thus improving the sintering of the coating. The second step was carried out in static air, to re-oxidise the spinel.

2) Simulated joining treatment: the coating was not sintered before the measurements. As possible sintering treatment, the consolidation/sealing treatment of the stack was used. In the case of ASR samples, where no consolidation of the stack was practically needed, this step was simulated reproducing the thermal profile of a real stack during the consolidation.

ASR test of small samples and samples preparation

In order to measure the ASR of the EPD coated plates, representative samples were cut from the centre of the plates. As a first step, on each plate lanthanum strontium manganite (LSM) cathode ribs were deposited, which would act as contact layer in a real stack between the interconnect of a single repeating unit and the cathode of the following one. This was made in order to simulate the stack operation. Squared coupons (2x2 cm^2) were cut from the EPD coated Crofer 22 APU plate. The

dimensions of the samples were chosen in order to have a representative position (i.e. presence of the cathode ribs, number of "crests and valleys" of the channelled surface). For each variant, two coupons were cut from the same plate. The electrical resistance was measured by using a four-terminal measurement. The electrical connection, needed to supply the current and to measure the voltage drop, was obtained by welding Pt-wires by point welding in correspondence of the valley of the channels. Before the welding, the coating and the oxide scale (in case of sintered coatings) were locally removed by precision abrasion to allow the welding of the wires. In order to exclude any artificial effects due to contacting with metallic meshes, a symmetrical assembly of two coupons was used. The cathode ribs were coated with a LSMC-based contact paste to establish a good electrical and mechanical contact between these two coupons.

The samples were subsequently placed in a muffle furnace Uhlig U24 for 5000 h in static air at 850 °C. Electric data was acquired by an Agilent 34970A data acquisition unit. The current was obtained measuring the voltage drop over a shunt. A current of 2 A was applied, which corresponds to a current density of 260 mA/cm².

Stack test

A 30-layer stack was built containing four repeating units with Mn-Co spinel coating deposited by EPD and sintered according to the two-step sintering procedure described above. The stack was tested in a double stack configuration for 3000 h, with a current density of 225 mA/cm², a hydrogen-nitrogen mixture as fuel gas with a fuel conversion rate of 75 %, at nominal 850 °C.

Characterization

Post-mortem morphological and chemical characterizations were carried out on the EPD coated plates submitted to the test in stack by means of SEM (SEM, Zeiss Merlin) equipped with an energy dispersive X-Ray analyser (EDX, Bruker) and transmission electron microscopy (TEM). FIB lamellae were prepared using NEON Cross-Beam 40EsB of ZEISS. High resolution TEM investigations were performed with Titan Cubed G2 60–300 (FEI) - a probe Cs corrected (S)TEM, equipped with ChemiSTEM EDX system based on a four windowless Silicon Drift Detectors (Super X). STEM imaging was performed in high angle annular dark-field mode (HAADF).

Results and Discussion

Small samples ASR results

The results of ASR measurements for both samples (sintered with two different treatments) up to 5000 h are reported in Figure 2. The sample subjected to the two-step sintering, after a small increase at the beginning of the test, shows a stable behaviour of the ASR which remains almost constant (~27mΩ cm^2) till 5000 h. On the other hand, the sample prepared with a simulated joining cycle shows a monotonic increase of the ASR and after the 5000 hours-test the value is found to be ~70 mΩ cm^2.

The ASR values at 5000 h for both types of samples together with the estimated degradation rate are summarised in Table 1. The degradation rate was estimated assuming a linear trend between 1000 h and 5000 h and then extrapolated from the slope of the linear fitting. Despite the ASR values at the beginning of the test are very close for both sets of samples, their difference become much more significant form 1000 h till the end of the test. Indeed, while a value of 28.1 mΩ cm^2 was recorded for the two-step sintered sample at the end of the test, 68.4 mΩ cm^2 is the final ASR value for the sample subjected to the simulated joining cycle as sintering treatment. The ASR degradation rate calculated in the case of two-step sintering is ≈0.5 mΩ cm^2 kh^{-1}. This value is less than one half of the value recorded for the same type of coating obtained by EPD but sintered only in air (1.2 mΩ cm^2 kh^{-1}) in a previous study [16] and 17 times lower than the degradation rate of the samples treated by simulated joining. From these data, it is apparent that the simulated joining cycle was not adequate to obtain satisfying performance from the coating, likely due to a low degree of densification.

The almost constant ASR value of the two-step sintered samples between the 2000 – 5000 hours is a remarkable data. Due to constant growth of the chromia oxide scale, especially at relatively high temperature of ~850 °C, an increase of the ASR could be expected. The observed stable level might be caused by several factors, including the conductivity increase of the LSM contact used due to sintering, masking the ASR increase of the coated interconnect. Also, instead of forming a Cr_2O_3 scale, Cr might be reacting with the spinel, thus forming high resistance compounds. From these data, we can exclude the formation of reaction products with high resistance and an excessive continuous growth of the oxide scale during the test. On the basis of these results the 2two-step sintering treatment was selected as post deposition treatment to be performed on IC plates coated by EPD and to be tested in the stack, as discussed in the following section.

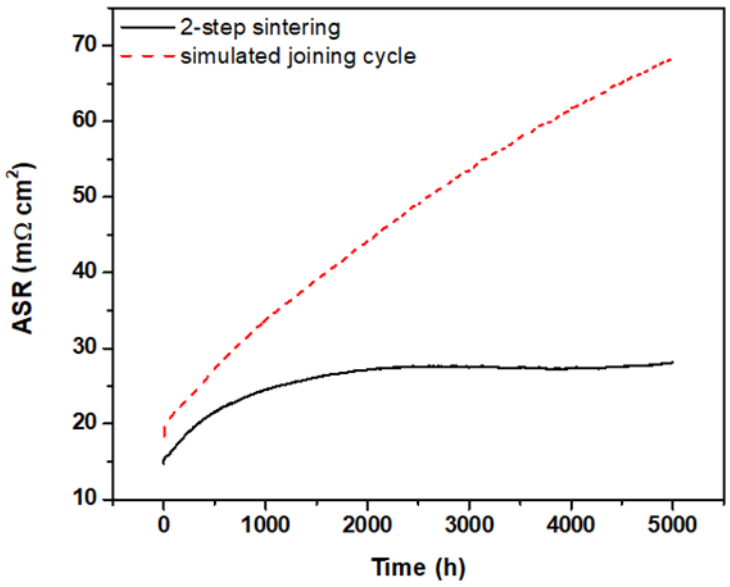

Figure 2: ASR values up to 5000 h at 850 °C in static air, of two samples sintered by two-step sintering (continuous line) and during the simulated joining cycle (dotted line).

Table 1: ASR values after 5000 h of test and estimated degradation rate of the samples reported in Figure 1.

	ASR after 5kh (mΩ cm²)	Degradation rate (mΩ cm² kh⁻¹)
Mn-Co-EPD Two-step sintering	28.1	0.5
Mn-Co-EPD Simulated joining cycle	68.4	8.7

Stack test and post-mortem analyses

Figure 3 shows the comparison between the ASR recorded for the single repeating unit (SRU) coated by EPD and sintered by two-step sintering and the one recorded for an SRU with the interconnect coated by the standard process used industrially by Sunfire GmbH. It needs to be specified that the ASR values reported here include the cell as well as the interconnect with coatings. The used cells were the same, thus the presented difference can be attributed to the different interconnects. The initial ASR for the SRU including the EPD coated interconnect is slightly (5-10 mΩ cm^2) lower than the reference one. Though the specific cell ASR is not known and thus cannot be easily accounted for, the typical values of the ASR usually obtained for planar interconnects with Mn-Co spinel EPD coatings are <30 mΩ cm^2 at these conditions [16], the improvement in interconnect performance of ~5-10 mΩ cm^2 can be considered quite substantial. Moreover, the difference between the recorded ASR values slowly change in favour for the SRU with EPD coated interconnect. The value

of difference goes from 0 to -10 mΩ cm^2 at the end of the test. This suggests a more stable performance in the case of interconnects coated by EPD and sintered with the two-step procedure. Also, the ASR value of the SRU containing the EPD coated interconnect stabilized in the last 500 h of the measurement, consistent with stabilization of ASR value of ex-situ tested EPD coated interconnect. These results, though obtained on a complex SRU platform, confirm the results obtained on ex-situ ASR tests and validate the EPD process in comparison with the one typically used in industrial applications.

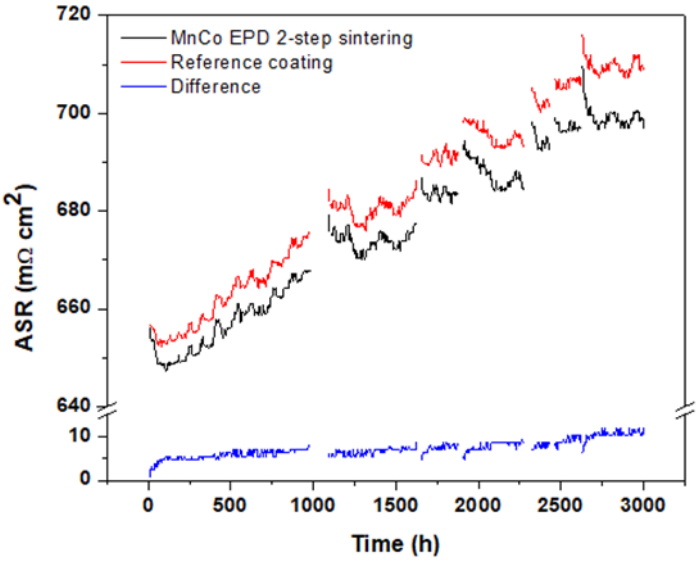

Figure 3: ASR of single repeating units tested in the stack coated with MnCo by EPD and subjected to two-step sintering (black curve) and coated with the standard coating used in Sunfire used as reference (red curve).

A schematic diagram showing the top view of the interconnects from the cathode side is reported in Figure 4a. The blue area represents the Mn-Co spinel coating. The portion of the Crofer 22 APU interconnect in contact with the cell is shaped by crests and valleys, as horizontal black lines in the picture; crests are partly coated by the cathode ribs in an alternate pattern. Four Crofer 22 APU Steel/Mn-Co spinel coating Interfaces (SCI) at the cathode side are considered in this study and outlined in Figure 4b:

1) SCI1: interface at the crest and under cathode rib (in direct electrical contact with the cell);
2) SCI2: interface at the oblique side (not in direct electrical contact with the cell);
3) SCI3: interface in the valley (not in direct electrical contact with the cell);

4) SCI4: interface at the crest without cathode rib (not in direct electrical contact with the cell).

Each prepared sample shows all the four SCIs (Figure 4c).

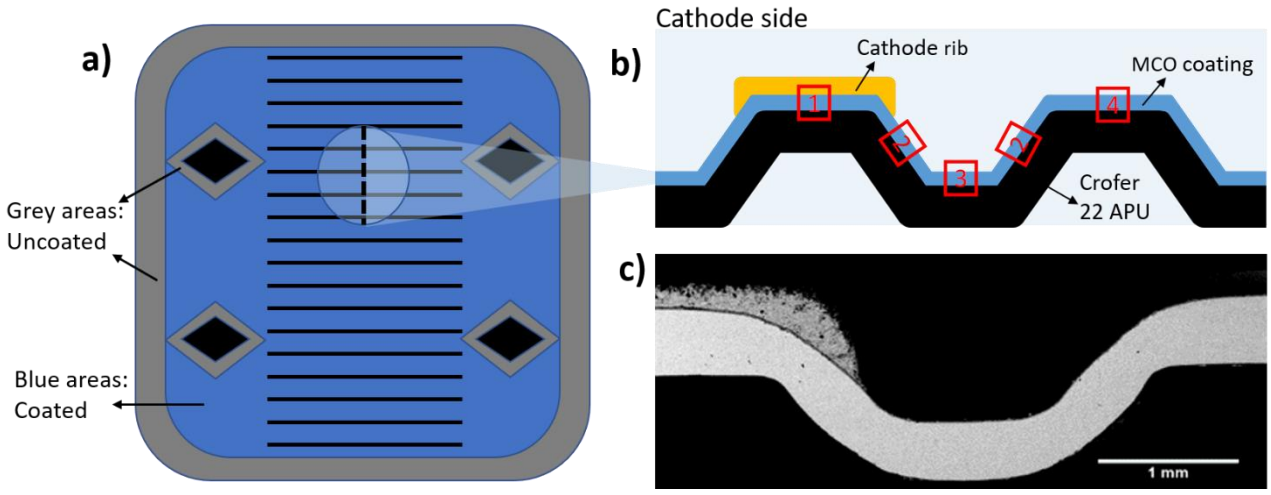

Figure 4: Schematic diagram (not-to-scale representation) of the coated interconnect (a) and cross section (b) with detail of four relevant interfaces (marked in red); c) SEM cross section overview of the coated interconnect.

The regions of the interconnects identified here as SCI 1 (crests under the cathode ribs) are those with the highest relevance, since the electrical polarization and the mechano-chemical interaction with the rib material can influence the evolution of this interface during the operation of the stack. In Figure 5, SEM backscattered images of SCI 1 with different magnification are provided; the interface between the coating and the cathode rib is clearly visible. Due to the contrast difference in the backscattered mode of the SEM, the different phases are clearly distinguishable in Figure 5b (from the bottom: steel, oxide scale, coating and LSM rib). Even after 3000 h at 850 °C, the coating appears generally homogeneous for thickness and morphology, thus confirming the good performance of the EPD method to cover the convex shapes of a Crofer 22 APU channelled surface. A thickness of 19±2 µm was measured for the Mn-Co coating. The porosity is uniformly distributed throughout the protective layer. No defects, cracks, delamination or spallation are visible at different interfaces. Furthermore, the cathode rib appears to be well adherent to the Mn-Co -spinel coating both on the top and on the oblique portion of the crest (right portion of Figure 5a). An excellent thermo-mechanical compatibility coating/steel and coating/rib is evaluated.

The development of a densified layer between the coating and the oxide scale is often reported for the oxidation of Crofer 22 APU with Mn-Co spinel coatings deposited by EPD [16,20,21,40]. This densified layer is generally defined as reaction layer, as it is the result of the interdiffusion of elements (Mn, Co, Cr) between the coating and the oxide scale during aging [8]. However, in this case, the densified layer is very thin (Figure 5b). The oxide scale presents irregular thickness and sub scale oxides. Such morphology is widely reported for the high-temperature oxidation of Crofer 22 APU [40,41]. The thickness of the oxide scale evaluated by SEM images analysis is 2.1±0.6 µm, which is coherent with previous finding in similar studies [16]. The oxide scale thickness can be considered low taking into account the exposure temperature. Already during the two-step sintering of the coatings, an initial >1µm thick oxide scale forms. Thus, the real oxide scale thickness increase caused by the subsequent 3000h exposure is ~1µm, which is considerably low and consistent with low ASR value.

The SEM cross section showed no indication of reactions during the stack test throughout the analysed regions, hence suggesting excellent long-term chemical compatibility of the Mn-Co coating with both the LSM contact layer and the Crofer 22 APU interconnect.

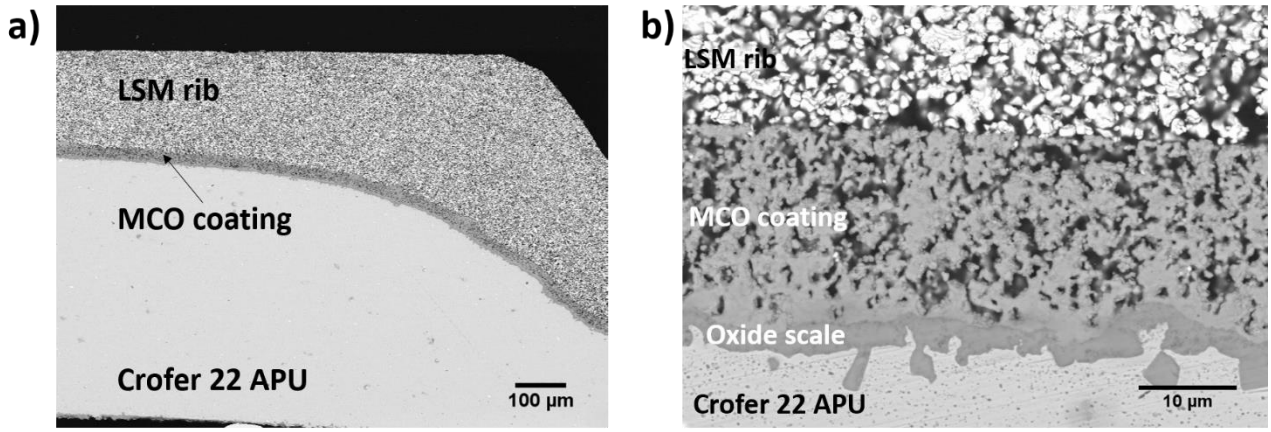

Figure 5: SEM backscattered images with different magnification of SCI 1 on samples collected from the stack test.

A more detailed post-mortem characterization of SCI 1 was carried out by transmission electron microscopy; the results are summarized in Figures 6 and 7.

Figure 6 shows a dark field STEM image (a) with STEM-EDX elemental maps (b-f) of the FIB lamella at SCI1. The chromium map (Figure 6b) clearly displays that Cr is completely confined in the oxide

scale, thus confirming the absence of a reaction layer. The scale seems to be constituted almost completely by pure Cr_2O_3, with the presence of Mn in some grains (due to diffusion from the steel or the coating). No Fe was detected in the scale. As anticipated, previous studies have indicated the presence of a reaction layer between the scale and the coating [8,16]. Molin et al reported the formation of ≈0.5 µm thick reaction layer after an aging of 5000 h at 800 °C in air. In this case the coating was obtained by EPD as well but sintered with a single step sintering process in oxidising atmosphere (air) [16]. On the other hand, Magdefrau et al. [8] reported a ≈ 4 µm layer thickness after 1000 h of aging at 800 °C. Despite the use of a reducing step in the sintering of the coating in this case, the thickness of the coating itself was lower (≈5 µm) compared with the present study and was deposited by screen-printing. The formation of mixed spinels $(Mn,Co,Cr)_3O_4$ in the coating side has to be considered disadvantageous due to the lower electrical conductivity of these species in comparison with a pure Mn-Co spinel.

Moreover, the Mn map (Figure 6e) reveals that the sub-scale oxide nodules developed during the test are rich in Mn and Cr. Other kind of internal oxidation is visible in the EDX maps of oxygen (d) and iron (f); elemental analysis confirmed that it corresponds to titanium oxide (the Ti map is not reported here).

Only manganese, cobalt and oxygen were identified in the coating region, thus confirming the high Cr-retention of the Mn-Co coating. However, the comparison of the Mn and Co maps shows that these two elements are not uniformly distributed throughout the coating. The same microstructure for similar Mn-Co spinel coatings was already described in a previous study [21]. This is due to the dual composition of the spinel: Mn_2CoO_4 and $MnCo_2O_4$. This behaviour is better visible in Figure 7 and will be discussed accordingly. On the other hand, oxygen concentration results homogeneous throughout the coating, suggesting the retention of the spinel structure and the absence of secondary phases.

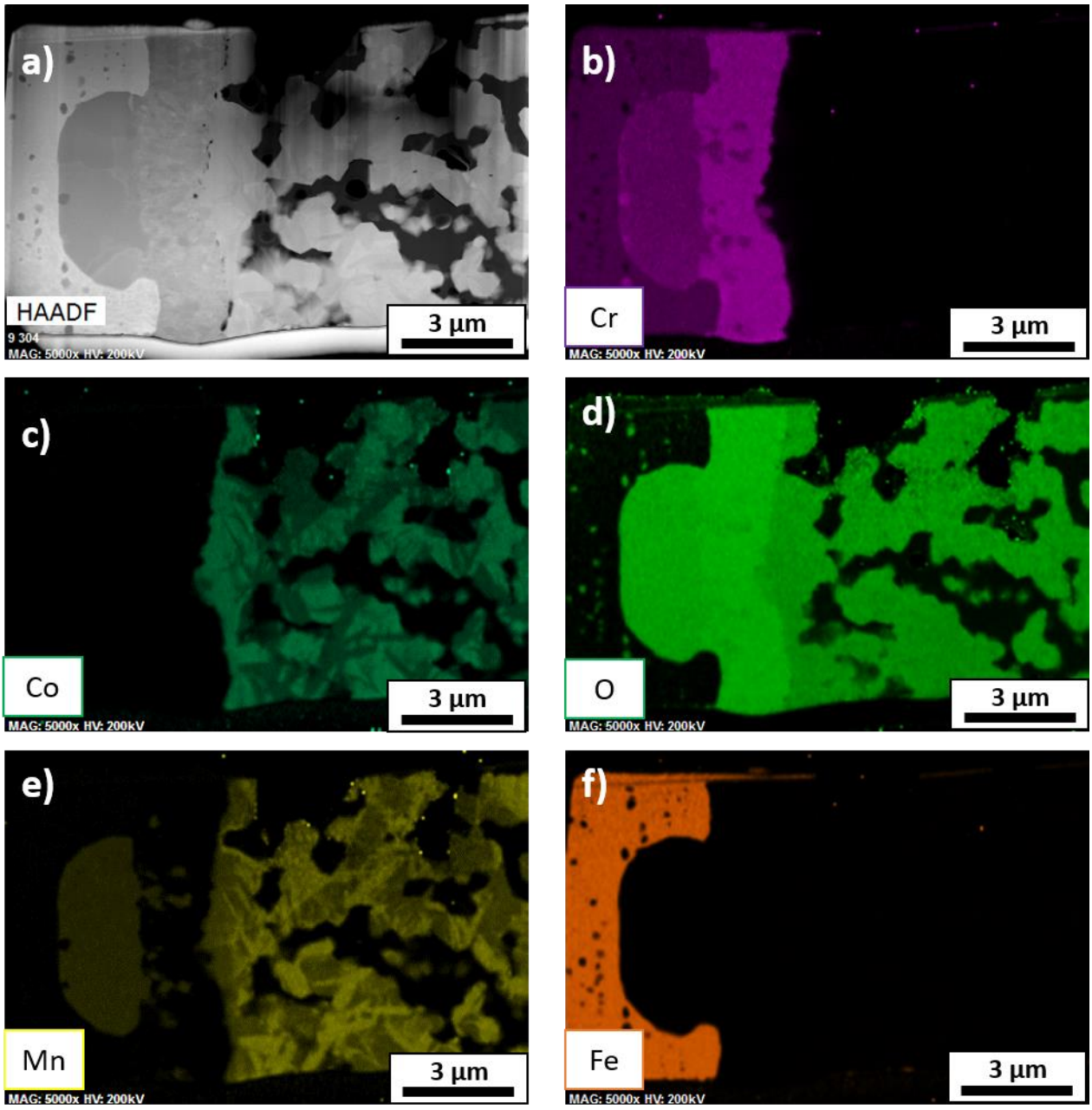

Figure 6: Transmission electron microscopy images of the FIB lamella: HAADF image with EDS elemental analysis (a–f).

Bright field TEM images with different magnification of the same FIB lamella are presented in Figure 7a and b, whereas a STEM-EDX map of the marked area is reported in Figure 7c. EDX elemental analysis results of numbered area and points are reported in the same figures.

The microstructure of the sub-scale nodule shown in Figure 7a is characterized by wide grains, rich in chromium and manganese. The Cr/Mn ratio obtained by EDX analysis (Area 1) fairly matches with

a Cr_2MnO_4 spinel. On the other hand, it is apparent that the oxide scale presents a completely different microstructure, as it is formed by packed and small grains (Figure 7b).

EDX analysis performed on some grains of oxide scale revealed the presence of Mn: 10 at.% in point 2 and ≈2 at.% in the adjacent grain (number 3). The manganese presence in the oxide scale is relevant as it can remarkably increase the electric conductivity thanks to the higher conductivity of the $(Mn,Cr)_3O_4$ spinel compared to pure chromia [42] and since $(Mn,Cr)_3O_4$ solid solutions phase has a lower Cr evaporation rate than Cr_2O_3 [43]. In this regard, manganese could diffuse into the scale during long term aging either from the steel or from the coating. In the first case, manganese can easily diffuse through the grain boundaries of the growing oxide scale during high-temperature oxidation [44]. Nevertheless, the second hypothesis seems to be more consistent with the EDX results, showing a Mn depletion from the grains of the coating in contact with the oxide scale.

The grains of the coating which are in direct contact with the oxide scale are generally wider compared to those in the central part of the coating. Indeed, just ≈300nm far from interface with the oxide scale, the Mn-Co spinel coating exhibits the same microstructure described in Ref. [21]; it is characterized by Mn-rich elongated grains surrounding Co-rich grains, as it is clearly visible in the EDX map reported 7c. It is worth to note that the Co/Mn ratios reported in Figure for points 6 and 7 almost perfectly fit with those required for the $MnCo_2O_4$ and tetragonal Mn_2CoO_4 spinel structure, respectively. This finding was expected, since the nominal $Mn_{1.5}Co_{1.5}O_4$ composition of the spinel is well known to contain both the structures Mn_2CoO_4 (tetragonal at room temperature) and $MnCo_2O_4$ (cubic) [9].

Tiny voids are visible at the interface between the oxide scale and the coating, well shown in Figure 7a and b. Having a maximum size of about 100 nm, these pores follow the boundary of the interface, but without initiating cracks. The pores are likely due to the different diffusion rates of Mn and Cr cations at the interface, according to the so called Kirkendall effect [44]. The EDS analyses confirmed a faster Mn diffusion from the coating towards the scale in comparison with Cr diffusion from the scale towards the coating (which results to be absent). This can be enhanced by the presence of the LSM rib which may act as Mn reservoir. Although there is a lack of research on this field, a possible electro migration effect in the Mn/Cr couple cannot be excluded as well [46].

It must be highlighted that porosity at the oxide scale/Mn-Co coating interface is not considered to be harmful or detrimental for long term operation in stack. To this purpose, the stack compression promoted a good adhesion and demonstrated to avoid possible delamination phenomena.

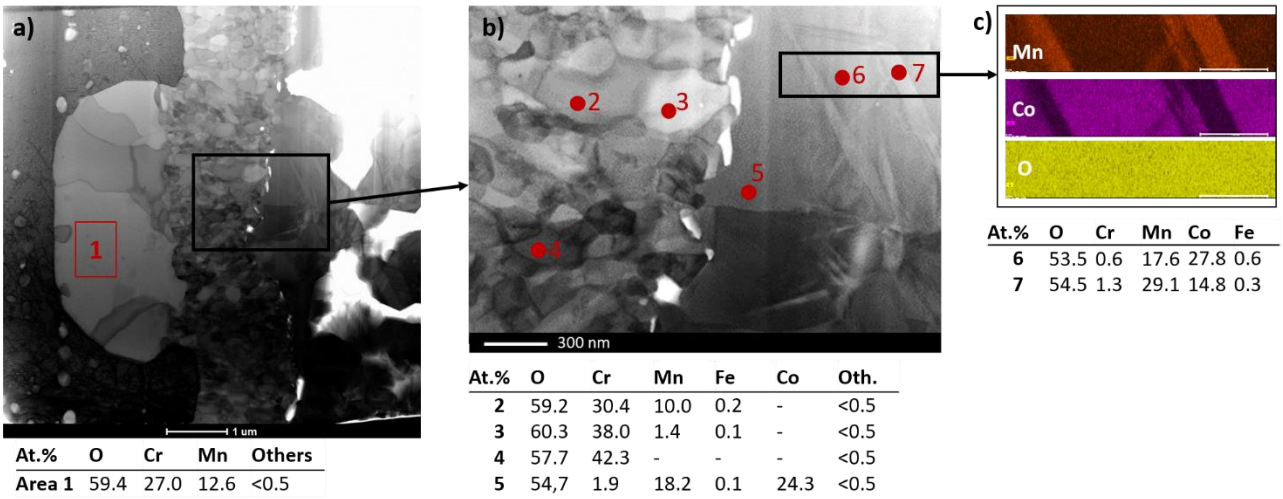

At.%	O	Cr	Mn	Others
Area 1	59.4	27.0	12.6	<0.5

At.%	O	Cr	Mn	Fe	Co	Oth.
2	59.2	30.4	10.0	0.2	-	<0.5
3	60.3	38.0	1.4	0.1	-	<0.5
4	57.7	42.3	-	-	-	<0.5
5	54,7	1.9	18.2	0.1	24.3	<0.5

At.%	O	Cr	Mn	Co	Fe
6	53.5	0.6	17.6	27.8	0.6
7	54.5	1.3	29.1	14.8	0.3

Figure 7: Transmission electron microscopy images of the FIB lamella and EDS elemental composition of marked area and points: BF TEM images at different magnification (a and b) and EDS map of marked region (c).

Morphological and chemical investigations were carried out also at different sites of the coated interconnect (see experimental section and Figure 4). Figure 8 shows SEM cross section images and EDX line scans (as marked by the arrows) respectively of SCI2 (Figure 8a and b), SCI3 (Figure 8c and d) and SCI4 (Figure 8e and f). The coating appears as a homogeneous layer in all the three cases. This evidence is especially relevant in the case of SCI2 (the oblique side) and SCI3 (the valley): indeed, due to the tilted position and the higher distance from the electrodes respectively, SCI2 and SCI3 could be subjected to a shadowing effect, resulting in poor, inhomogeneous deposition. Selecting a deposition method able to guarantee homogeneous coatings over the whole area of interconnects with complex shapes is a key element for high-efficiency stacks. To this purpose, EPD demonstrated to be an effective technique to deposit uniform coatings on complex channelled surfaces. In particular, the measured thickness on the coating at SCI2 (Figure 8a) and SCI3 (Figure 8c) is on average ≈17 µm and ≈15 µm respectively, slightly lower that of SCI1 discussed above. However, these thicknesses are still considered to be sufficiently high to guarantee an effective protective performance of the coating. Furthermore, no cracks are detected in any convex or concave region after the sintering, thus confirming the good selection of the sintering treatment related to the coating and its geometry. Indeed, as reported by Talic et al. [19], the sintering treatment may induce formation of cracks in stress accumulation points of a channelled surface. However, this effect is related not only to the deposition method and the sintering treatment, but also to the coating thickness and curvature radius of the corner in the channels.

The interface labelled SCI4 (Figure 8e) is the equivalent of SCI1 but without the application of LSM rib on the top. The thickness of the coating in this site resulted to be ≈21 µm which is comparable to the thickness observed in SCI1 (Figure 5). The higher thickness in SCI1 and SCI4 in comparison with SCI2 and SCI3 may be due to the fact that SCI1 and SCI4 were closer to the counter-electrode during the EPD process and so they were subjected to a higher flux of particles in comparison with SCI2 and SCI3. The characteristics of the oxide scale visible from the SEM images in Figure 8 are equivalent to those discussed regarding SCI1 in Figure 5. However, it is evident the presence of a densified coating layer in contact with the oxide scale both in SCI2 and SCI3; the outer part of the coating appears porous instead. It seems that the densified layer is partially visible also in SCI4. This supports the hypothesis that the microstructure of SCI1 is influenced by the electrical polarization and the interaction with the LSM rib, not present in the case of SCI2 SCI3 and SCI4. EDX line scans from each interface are reported in Figure 8 as well. Due to the EDX volume interaction, it is not possible to determine the thickness of the oxide scales and the nature of the reaction layer with great accuracy. Nevertheless, it is clear that the thickness of the oxide scale is in the range of 1-2 µm and that the chromium amount in the coating decreases to almost zero within few µm which indicates a very high Cr retention also in these regions of the interconnect.

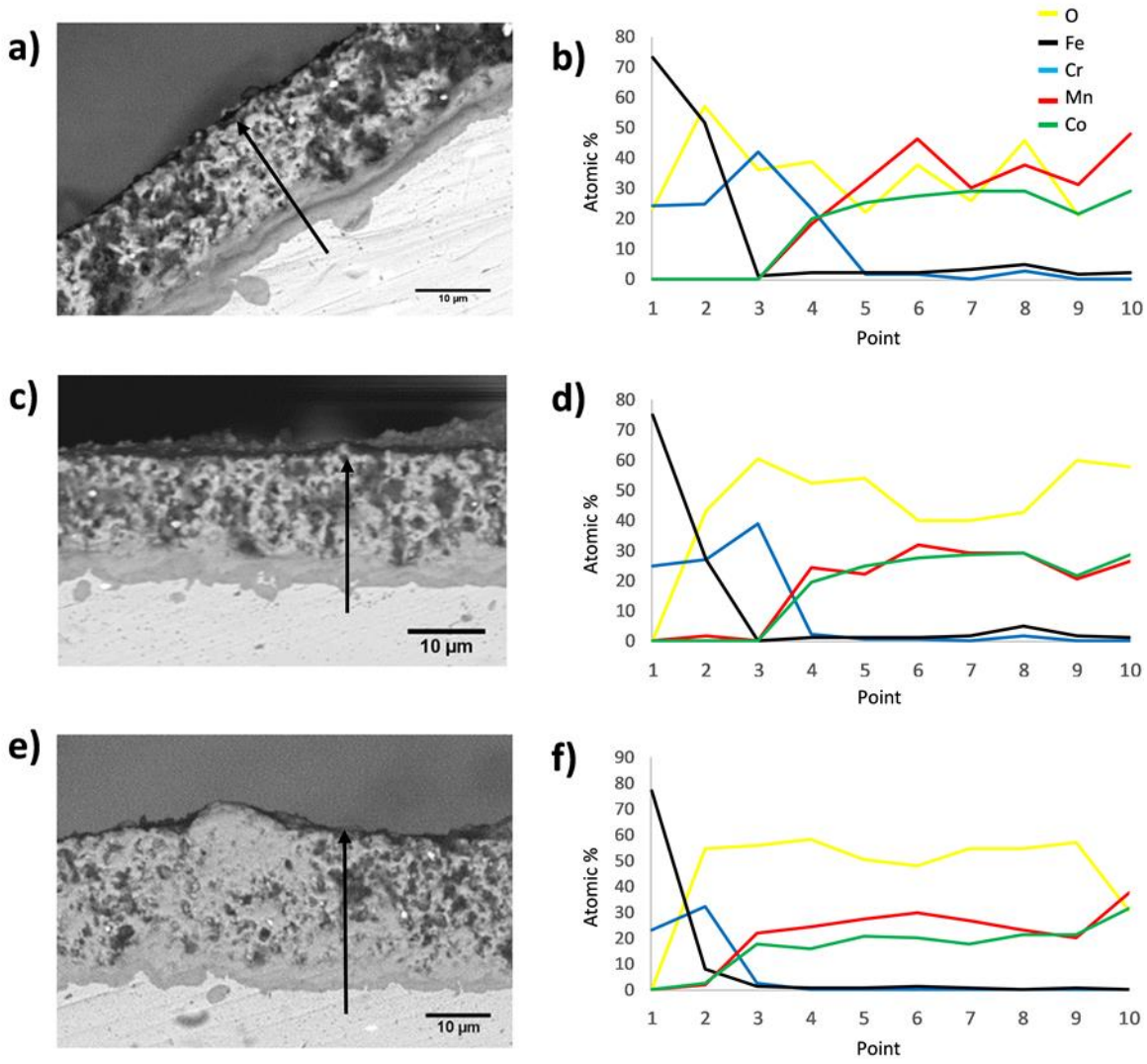

Figure 8. SEM cross section images (backscattered mode) and EDS line scans (marked by the arrows) of different sites of interest at the steel/coating interface: SCI2 (a and b), SCI3 (c and d), SCI4 (e and f).

Conclusions

This study has demonstrated that EPD can be used to coat real dimension interconnect plates with a Mn-Co spinel, achieving thickness reproducibility and homogeneity on different areas, both concave and convex ones. This can be considered to be a significant step forward in the use of EPD as versatile, low cost, easy and reproducible method in fuel cell technology, particularly to coat complex shapes on real scales. The SRU in which the IC was coated with EPD and subjected to two-step sintering demonstrated an ASR slightly lower to the reference SRU for all the duration of the stack tests. The post mortem analyses carried out after the stack test proved that the protective ceramic coating was an effective mass transport barrier against Cr diffusion from the Crofer 22 APU

together with an excellent limitation in the oxide scale growth. The coating resulted to have an excellent compatibility with both the steel and the LSM rib. No formation of detrimental compounds was detected after 3000 h of stack test together with a limited oxide scale growth, thus validating the ASR results. The morphological analyses pointed out a uniform deposition of real dimension plates on different sites of the channelled surface. In conclusion, the present study represents a proof of the suitability and maturity of EPD as an effective deposition technique for the processing of ceramic coatings on solid oxide cells interconnects.

Acknowledgments

F. S. and A. R. B. would like to acknowledge the KMM-VIN (http://www.kmm-vin.eu/home/fellowships) 11th call granted to E. Zanchi. This project has received funding from the European Union's Horizon 2020 research and innovation programme under grant agreement No 823717 – ESTEEM3.

References

[1] Z. Yang, M. Guo, N. Wang, C. Ma, J. Wang, M. Han, A short review of cathode poisoning and corrosion in solid oxide fuel cell, Int. J. Hydrogen Energy. 42 (2017) 24948–24959. https://doi.org/10.1016/j.ijhydene.2017.08.057.

[2] S. Fontana, S. Chevalier, G. Caboche, Metallic interconnects for solid oxide fuel cell: Effect of water vapour on oxidation resistance of differently coated alloys, J. Power Sources. 193 (2009) 136–145. https://doi.org/10.1016/j.jpowsour.2008.11.041.

[3] S. Chevalier, L. Combemale, I. Popa, S. Chandra-Ambhorn, W. Chandra-Ambhorn, P. Promdirek, P. Wongpromrat, Development of sofc interconnect stainless steels, Solid State Phenom. 300 (2020) 135–156. https://doi.org/10.4028/www.scientific.net/SSP.300.135.

[4] J.C.W. Mah, A. Muchtar, M.R. Somalu, M.J. Ghazali, Metallic interconnects for solid oxide fuel cell: A review on protective coating and deposition techniques, Int. J. Hydrogen Energy. 42 (2015) 9219-9229. https://doi.org/10.1016/j.ijhydene.2016.03.195.

[5] A. Petric, H. Ling, Electrical conductivity and thermal expansion of spinels at elevated temperatures, J. Am. Ceram. Soc. 90 (2007) 1515–1520. https://doi.org/10.1111/j.1551-2916.2007.01522.x.

[6] Z. Shen, J. Rong, X. Yu, $Mn_xCo_{3-x}O_4$ spinel coatings: Controlled synthesis and high temperature oxidation resistance behavior, Ceram. Int. 46 (2020) 5821–5827. https://doi.org/10.1016/j.ceramint.2019.11.032.

[7] B. Kamecki, J. Karczewski, T. Miruszewski, G. Jasiński, D. Szymczewska, P. Jasiński, S. Molin, Low temperature deposition of dense $MnCo_2O_4$ protective coatings for steel interconnects of solid oxide cells, J. Eur. Ceram. Soc. 38 (2018) 4576–4579. https://doi.org/10.1016/j.jeurceramsoc.2018.05.042.

[8] N.J. Magdefrau, L. Chen, E.Y. Sun, J. Yamanis, M. Aindow, Formation of spinel reaction layers in manganese cobaltite-coated Crofer22 APU for solid oxide fuel cell interconnects, J. Power Sources. 227 (2013) 318–326. https://doi.org/10.1016/j.jpowsour.2012.07.091.

[9] Z. Yang, G.G. Xia, X.H. Li, J.W. Stevenson, $(Mn,Co)_3O_4$ spinel coatings on ferritic stainless steels for SOFC interconnect applications, Int. J. Hydrogen Energy. 32 (2007) 3648–3654. https://doi.org/10.1016/j.ijhydene.2006.08.048.

[10] N. Grünwald, Y.J. Sohn, X. Yin, N.H. Menzler, O. Guillon, R. Vaßen, Microstructure and phase evolution of atmospheric plasma sprayed Mn-Co-Fe oxide protection layers for solid oxide fuel cells, J. Eur. Ceram. Soc. 39 (2019) 449–460, https://doi.org/10.1016/j.jeurceramsoc.2018.08.027.

[11] H. Falk-Windisch, J. Claquesin, M. Sattari, J.-E. Svensson, J. Froitzheim, Co- and Ce/Co-coated ferritic stainless steel as interconnect material for Intermediate Temperature Solid Oxide Fuel Cells, J. Power Sources. 343 (2017) 1–10. https://doi.org/10.1016/j.jpowsour.2017.01.045.

[12] C.C. Mardare, M. Spiegel, A. Savan, A. Ludwig, Thermally Oxidized Mn–Co Thin Films as Protective Coatings for SOFC Interconnects, J. Electrochem. Soc. 156 (2009) B1431. https://doi.org/10.1149/1.3240597.

[13] S.J. Han, Z. Pala, S. Sampath, Plasma sprayed manganese-cobalt spinel coatings: Process sensitivity on phase, electrical and protective performance, J. Power Sources. 304 (2016) 234–243. https://doi.org/10.1016/j.jpowsour.2015.11.040.

[14] J. Puranen, M. Pihlatie, J. Lagerbom, G. Bolelli, J. Laakso, L. Hyvärinen, M. Kylmälahti, O. Himanen, J. Kiviaho, L. Lusvarghi, P. Vuoristo, Post-mortem evaluation of oxidized atmospheric plasma sprayed Mn-Co-Fe oxide spinel coatings on SOFC interconnectors, Int. J. Hydrogen Energy. 39 (2014) 17284–17294. https://doi.org/10.1016/j.ijhydene.2014.08.105.

[15] L.C. Ajitdoss, F. Smeacetto, M. Bindi, D. Beretta, M. Salvo, M. Ferraris, $Mn_{1.5}Co_{1.5}O_4$ protective coating on Crofer 22 APU produced by thermal co-evaporation for SOFCs, Mater. Lett. 95 (2013) 82–85. https://doi.org/10.1016/j.matlet.2012.12.079.

[16] S. Molin, A.G. Sabato, M. Bindi, P. Leone, G. Cempura, M. Salvo, S. Cabanas Polo, A.R. Boccaccini, F. Smeacetto, Microstructural and electrical characterization of Mn-Co spinel protective coatings for solid oxide cell interconnects, J. Eur. Ceram. Soc. 37 (2017) 4781–4791. https://doi.org/10.1016/j.jeurceramsoc.2017.07.011.

[17] Q.X. Fu, D. Sebold, F. Tietz, H.P. Buchkremer, Electrodeposited cobalt coating on Crofer 22 APU steels for interconnect applications in solid oxide fuel cells, Solid State Ionics. 192 (2011) 376–382. https://doi.org/10.1016/j.ssi.2010.03.010.

[18] Q. Fu, F. Tietz, D. Sebold, E. Wessel, H.P. Buchkremer, Magnetron-sputtered cobalt-based protective coatings on ferritic steels for solid oxide fuel cell interconnect applications, Corros. Sci. 54 (2012) 68–76. https://doi.org/10.1016/j.corsci.2011.08.051.

[19] B. Talic, A.C. Wulff, S. Molin, K.B. Andersen, P. Zielke, H.L. Frandsen, Investigation of electrophoretic deposition as a method for coating complex shaped steel parts in solid oxide cell stacks, Surf. Coatings Technol. 380 (2019) 125093. https://doi.org/10.1016/j.surfcoat.2019.125093.

[20] B. Talic, S. Molin, K. Wiik, P. Vang, H. Lea, Comparison of iron and copper doped manganese cobalt spinel oxides as protective coatings for solid oxide fuel cell interconnects, 372 (2017) 145–156, https://doi.org/10.1016/j.jpowsour.2017.10.060.

[21] E. Zanchi, S. Molin, A.G. Sabato, B. Talic, G. Cempura, A.R. Boccaccini, F. Smeacetto, Iron doped manganese cobaltite spinel coatings produced by electrophoretic co-deposition on interconnects for solid oxide cells: Microstructural and electrical characterization, J. Power Sources. 455 (2020) 227910. https://doi.org/10.1016/j.jpowsour.2020.227910.

[22] H. Abdoli, P. Alizadeh, Electrophoretic deposition of $(Mn,Co)_3O_4$ spinel nano powder on SOFC metallic interconnects, Mater. Lett. 80 (2012) 53–55. https://doi.org/10.1016/j.matlet.2012.04.072.

[23] M. Bobruk, S. Molin, M. Chen, T. Brylewski, P. V Hendriksen, Sintering of $MnCo_2O_4$ coatings prepared by electrophoretic deposition, Mater. Letters 213 (2018) 394–398, https://doi.org/10.1016/j.matlet.2017.12.046.

[24] S. Molin, A.G. Sabato, H. Javed, G. Cempura, A.R. Boccaccini, F. Smeacetto, Co-deposition of CuO and $Mn_{1.5}Co_{1.5}O_4$ powders on Crofer 22 APU by electrophoretic method: structure, compositional modifications and corrosion properties, Mater. Letters 218 (2018) 329–333, https://doi.org/10.1016/j.matlet.2018.02.037.

[25] M. Mirzaei, A. Simchi, M.A. Faghihi-sani, A. Yazdanyar, Electrophoretic deposition and sintering of a nanostructured manganese – cobalt spinel coating for solid oxide fuel cell interconnects, Ceram. Int. 42 (2016) 1–9. https://doi.org/10.1016/j.ceramint.2016.01.012.

[26] A.G. Sabato, In-situ Cu-doped MnCo-spinel coatings for solid oxide cell interconnects processed by electrophoretic deposition, Ceram. Int. 45 (2019) 19148-19157, https://doi.org/10.1016/j.ceramint.2019.06.161.

[27] E. Zanchi, Electrophoretic co-deposition of Fe_2O_3 and $Mn_{1.5}Co_{1.5}O_4$: Processing and oxidation performance of Fe-doped Mn-Co coatings for solid oxide cell interconnects, J. Eur. Ceram. Soc. 39 (2019) 3768-3777, https://doi.org/10.1016/j.jeurceramsoc.2019.05.024.

[28] H. Zhang, Z. Zhan, X. Liu, Electrophoretic deposition of $(Mn,Co)_3O_4$ spinel coating for solid oxide fuel cell interconnects, J. Power Sources. 196 (2011) 8041–8047. https://doi.org/10.1016/j.jpowsour.2011.05.053.

[29] Z. Sun, S. Gopalan, U.B. Pal, S.N. Basu, Electrophoretically Deposited Copper Manganese Spinel Coatings for Prevention of Chromium Poisoning in Solid Oxide Fuel Cells, in: T. Wang, X. Chen, D.P. Guillen, L. Zhang, Z. Sun, C. Wang, N. Haque, J.A. Howarter, N.R. Neelameggham, S. Ikhmayies, Y.R. Smith, L. Tafaghodi, A. Pandey (Eds.), Energy Technol. 2019, Springer International Publishing, Cham, 2019: pp. 265–272.

[30] Z. Sun, S. Gopalan, U.B. Pal, S.N. Basu, $Cu_{1.3}Mn_{1.7}O_4$ spinel coatings deposited by electrophoretic deposition on Crofer 22 APU substrates for solid oxide fuel cell applications, Surf. Coatings Technol. J. in press 323 (2016) 49-57. https://doi.org/http://dx.doi.org/10.1016/j.surfcoat.2016.09.028.

[31] W. Huang, S. Gopalan, U.B. Pal, S.N. Basu, Evaluation of Electrophoretically Deposited $CuMn_{1.8}O_4$ Spinel Coatings on Crofer 22 APU for Solid Oxide Fuel Cell Interconnects, J. Electrochem. Soc. 155 (2008) B1161. https://doi.org/10.1149/1.2975367.

[32] J. Yoo, S.K. Woo, J.H. Yu, S. Lee, G.W. Park, $La_{0.8}Sr_{0.2}MnO_3$ and $(Mn_{1.5}Co_{1.5})O_4$ double layer coated by electrophoretic deposition on Crofer22 APU for SOEC interconnect applications, Int. J. Hydrogen Energy. 34 (2009) 1542–1547. https://doi.org/10.1016/j.ijhydene.2008.12.005.

[33] M. Palcut, L. Mikkelsen, K. Neufeld, M. Chen, R. Knibbe, P.V. Hendriksen, Improved oxidation resistance of ferritic steels with LSM coating for high temperature electrochemical applications, Int. J. Hydrogen Energy. 37 (2012) 8087–8094. https://doi.org/10.1016/j.ijhydene.2011.11.138.

[34] S. Hu, W. Li, H. Finklea, X. Liu, A review of electrophoretic deposition of metal oxides and its application in solid oxide fuel cells, Adv. Colloid Interface Sci. 276 (2020) 102102. https://doi.org/10.1016/j.cis.2020.102102.

[35] B. Talic, H. Falk-Windisch, V. Venkatachalam, P. Vang Hendriksen, K. Wiik, H. L. Lein, Effect of coating density on oxidation resistance and Cr vaporization from solid oxide fuel cell

interconnects, J. Power Sources 354 (2017) 57-67. http://dx.doi.org/10.1016/j.jpowsour.2017.04.023.

[36] L. Besra, M. Liu, A review on fundamentals and applications of electrophoretic deposition (EPD), Prog. Mater. Sci. 52 (2007) 1–61. https://doi.org/10.1016/j.pmatsci.2006.07.001.

[37] A.R. Boccaccini, I. Zhitomirsky, Application of electrophoretic and electrolytic deposition techniques in ceramics processing, Current Opinion in Solid State and Materials Science 6 (2002) 251-260. https://doi.org/10.1016/S1359-0286(02)00080-3.

[38] N.H. Menzler, D. Sebold, O. Guillon, Post-test characterization of a solid oxide fuel cell stack operated for more than 30,000 hours: The cell, J. Power Sources. 374 (2018) 69–76. https://doi.org/10.1016/j.jpowsour.2017.11.025.

[39] M. Bianco, J.P. Ouweltjes, J. Van herle, Degradation analysis of commercial interconnect materials for solid oxide fuel cells in stacks operated up to 18000 hours, Int. J. Hydrogen Energy. 44 (2019) 31406–31422. https://doi.org/10.1016/j.ijhydene.2019.09.218.

[40] S. Molin, P. Jasinski, L. Mikkelsen, W. Zhang, M. Chen, P. V. Hendriksen, Low temperature processed $MnCo_2O_4$and $MnCo_{1.8}Fe_{0.2}O_4$ as effective protective coatings for solid oxide fuel cell interconnects at 750°C, J. Power Sources. 336 (2016) 408–418. https://doi.org/10.1016/j.jpowsour.2016.11.011.

[41] B. Talic, S. Molin, P.V. Hendriksen, H.L. Lein, Effect of pre-oxidation on the oxidation resistance of Crofer 22 APU, Corros. Sci. 138 (2018) 189–199, https://doi.org/10.1016/j.corsci.2018.04.016.

[42] Z. Lu, J. Zhu, E. Andrew Payzant, M.P. Paranthaman, Electrical conductivity of the manganese chromite spinel solid solution, J. Am. Ceram. Soc. 88 (2005) 1050–1053. https://doi.org/10.1111/j.1551-2916.2005.00205.x.

[43] C. Gindorf, L. Singheiser, K. Hilpert, Chromium vaporisation from Fe, Cr base alloys used as interconnect in fuel cells, Steel Res. 72 (2001) 528–533. https://doi.org/10.1002/srin.200100163.

[44] Z. Yang, G.G. Xia, C.M. Wang, Z. Nie, J. Templeton, J.W. Stevenson, P. Singh, Investigation of iron-chromium-niobium-titanium ferritic stainless steel for solid oxide fuel cell interconnect applications, J. Power Sources. 183 (2008) 660–667.

[45] K.-N. Tu, A.M. Gusak, Kirkendall effect and inverse kirkendall effect, Chapter 3, in: Kinet. Nanoscale Mater., 2nd ed., John Wiley & Sons, Incorporated, 2014: pp. 67–98.

[46] D. Kim, J.C. Jungil, Formation and behavior of Kirkendall voids within intermetallic layers of solder joints, J. Mater. Sci. Mater. Electron. 22 (2011) 703–716. https://doi.org/10.1007/s10854-011-0357-2.

Table 1

	ASR after 5kh (mΩ cm^2)	Degradation rate (mΩ cm^2 kh^{-1})
Mn-Co-EPD Two-step sintering	28.1	0.5
Mn-Co-EPD Simulated joining cycle	68.4	8.7

Figure 1

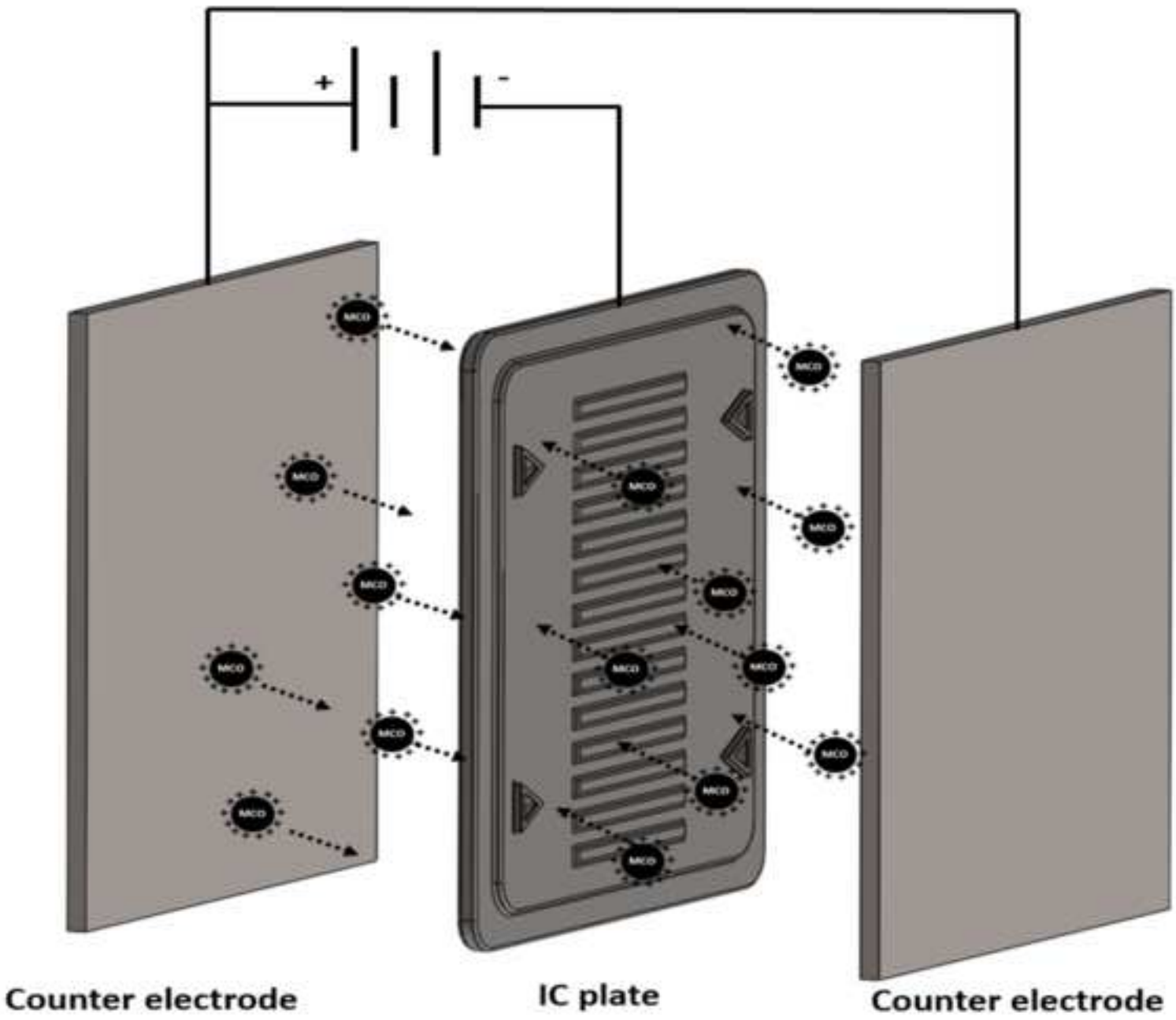

Figure 2

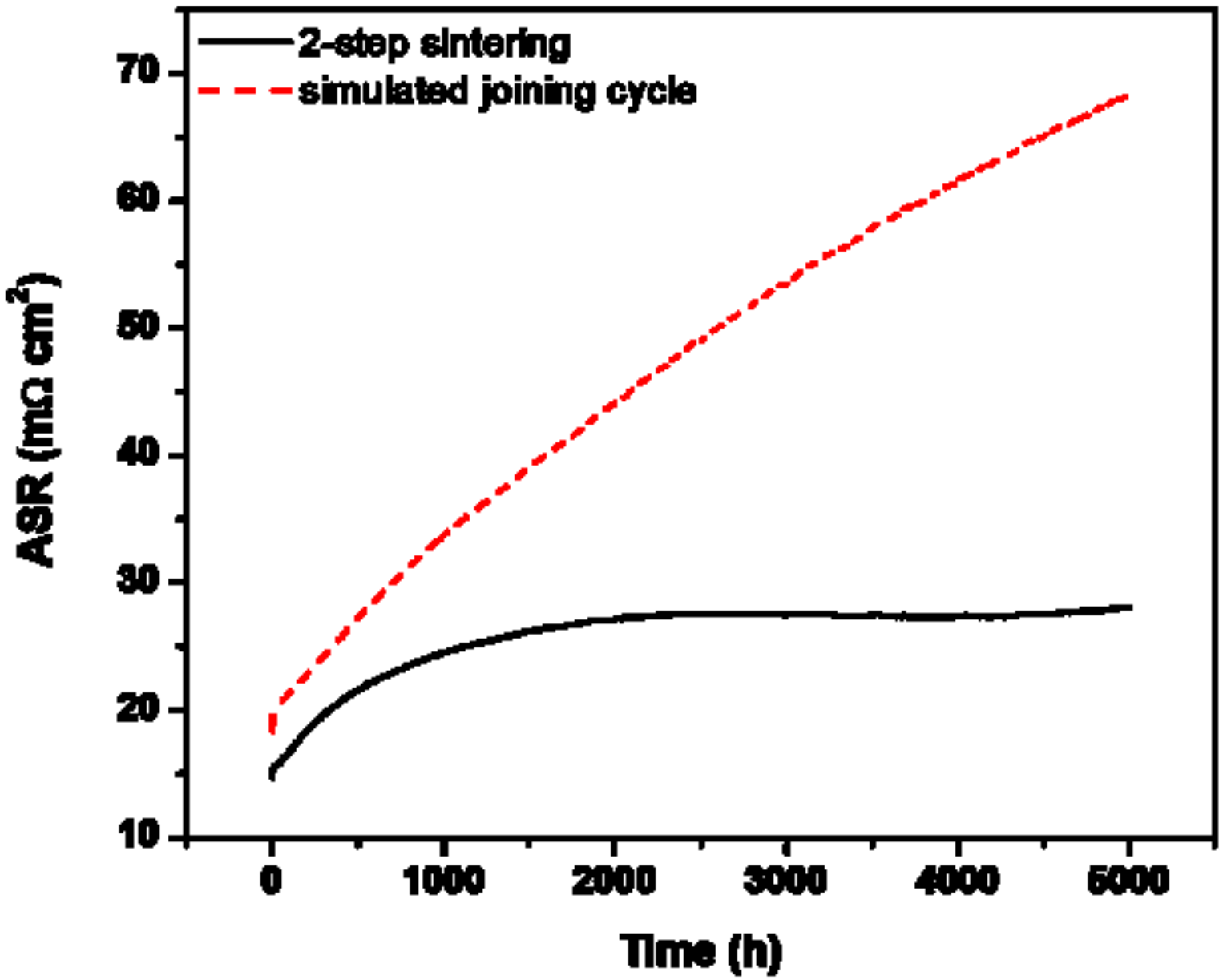

Figure 3

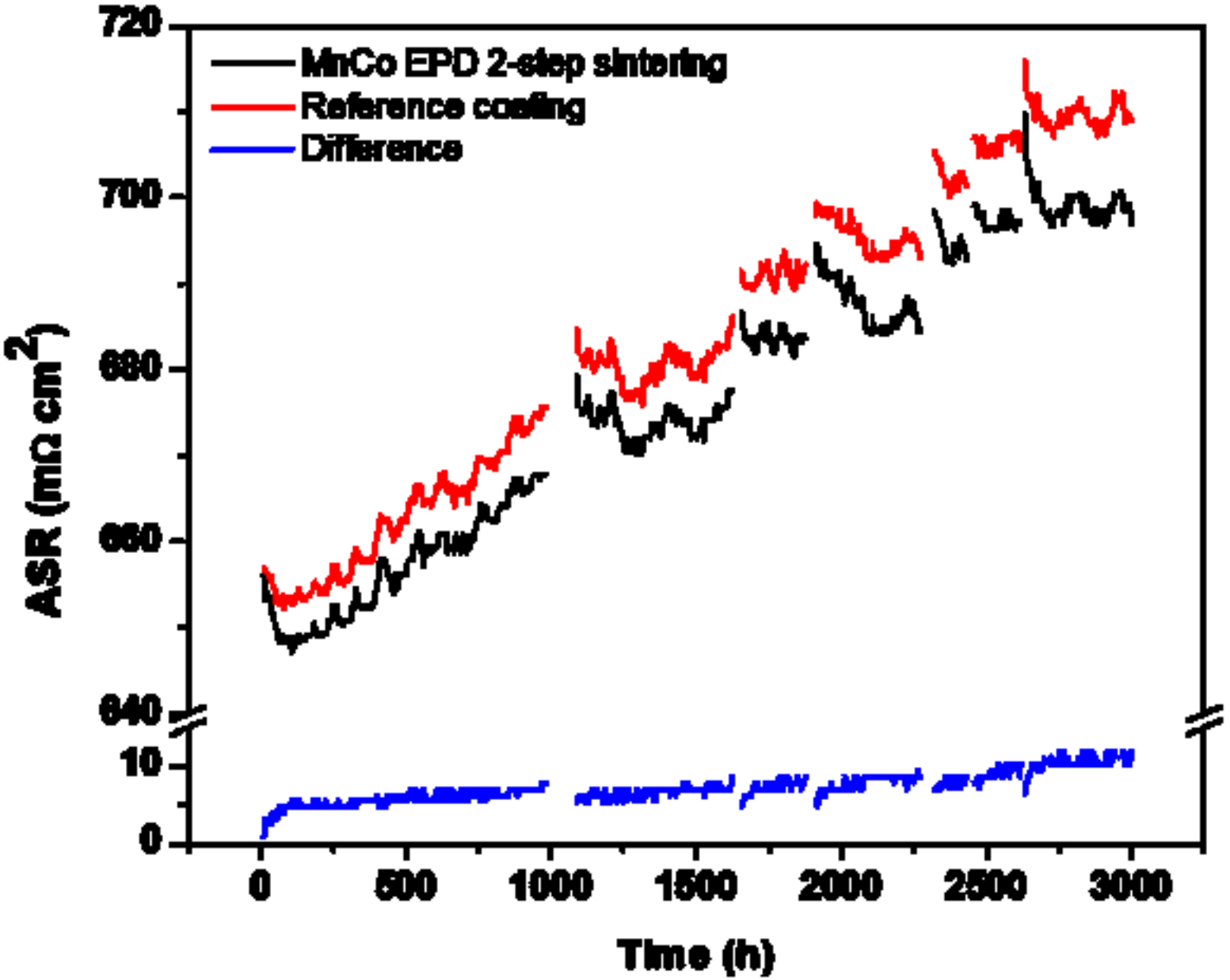

Figure 4

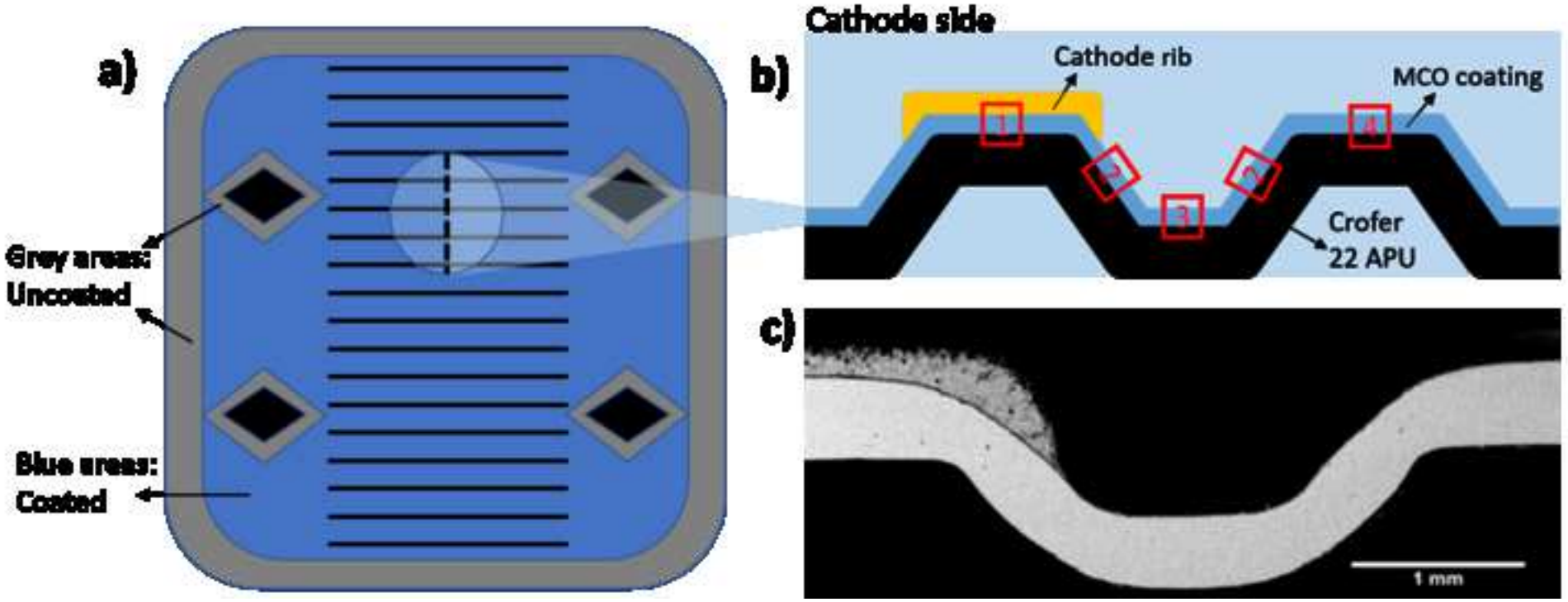

Figure 5

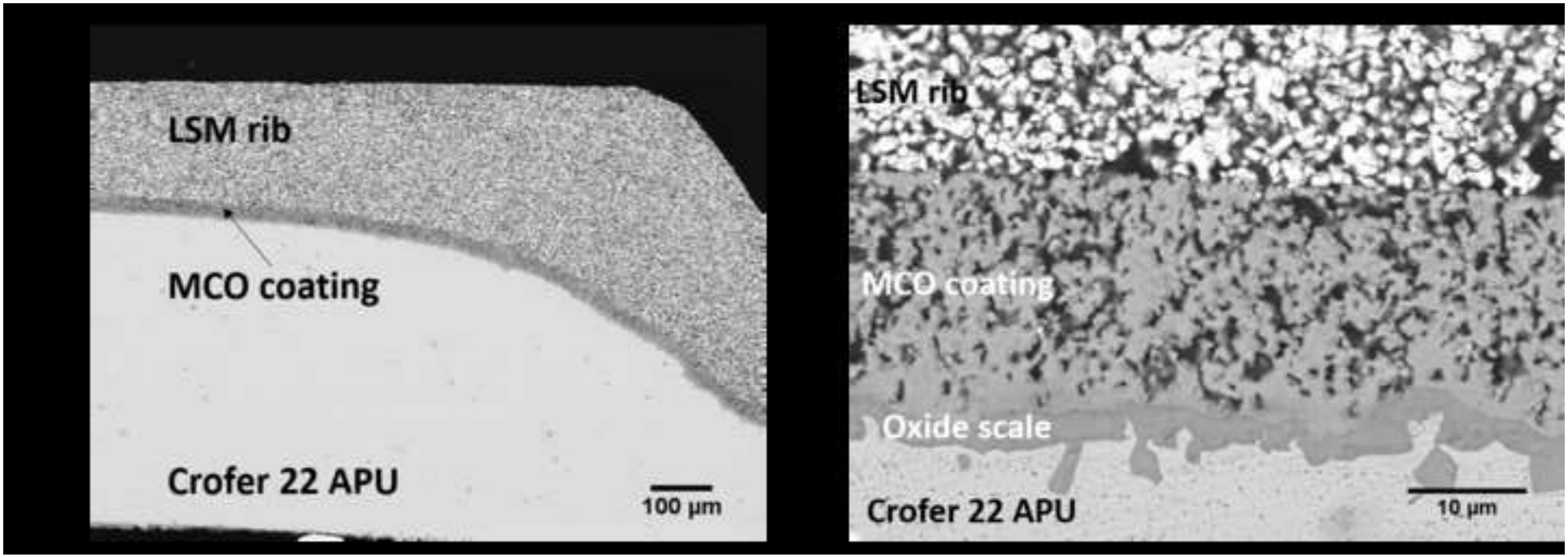

Figure 6

Click here to access/download;Figure;Fig. 6.tif

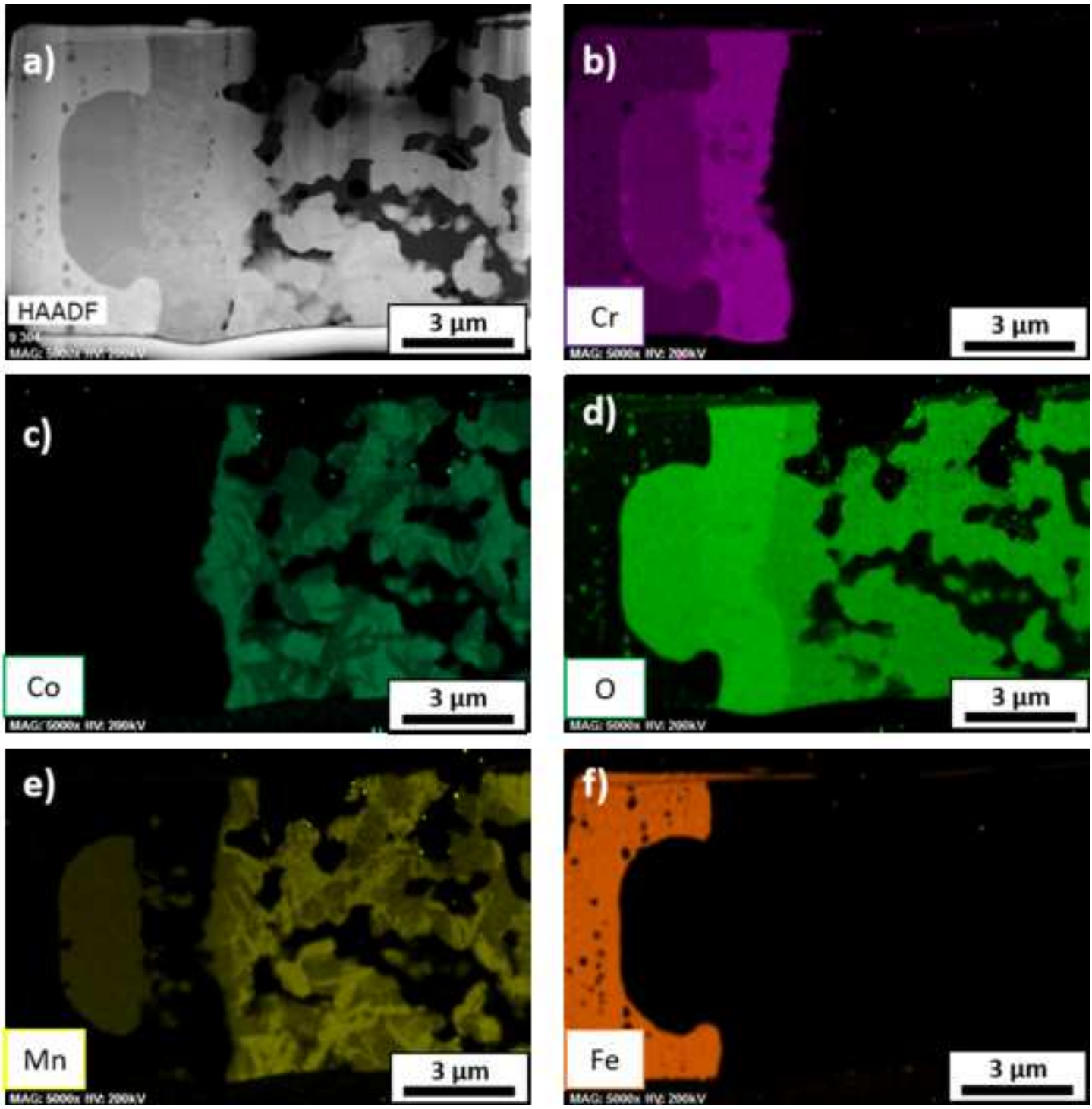

Figure 7

Click here to access/download;Figure;Fig. 7.png

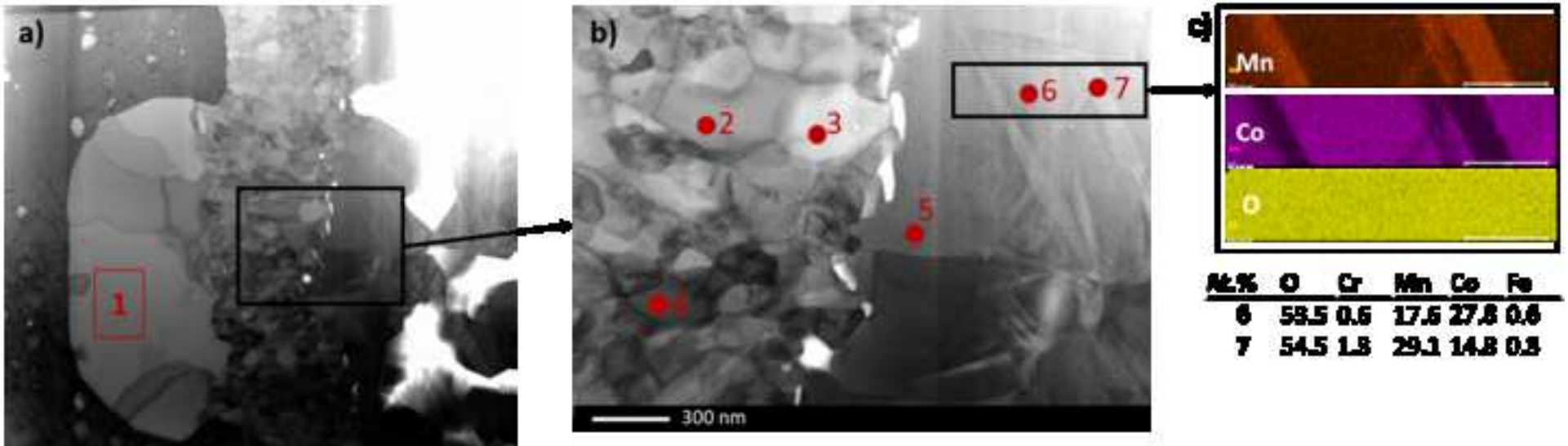

At.%	O	Cr	Mn	Others
Area 1	59.4	27.0	12.6	<0.5

At.%	O	Cr	Mn	Fe	Co	Others
2	59.2	30.4	10.0	0.2	-	<0.5
3	60.3	38.0	1.4	0.1	-	<0.5
4	57.7	42.3	-	-	-	<0.5
5	54.7	1.9	18.2	0.1	24.3	<0.5

At.%	O	Cr	Mn	Co	Fe
6	58.5	0.6	17.6	27.8	0.6
7	54.5	1.8	29.1	14.8	0.8

Figure 8

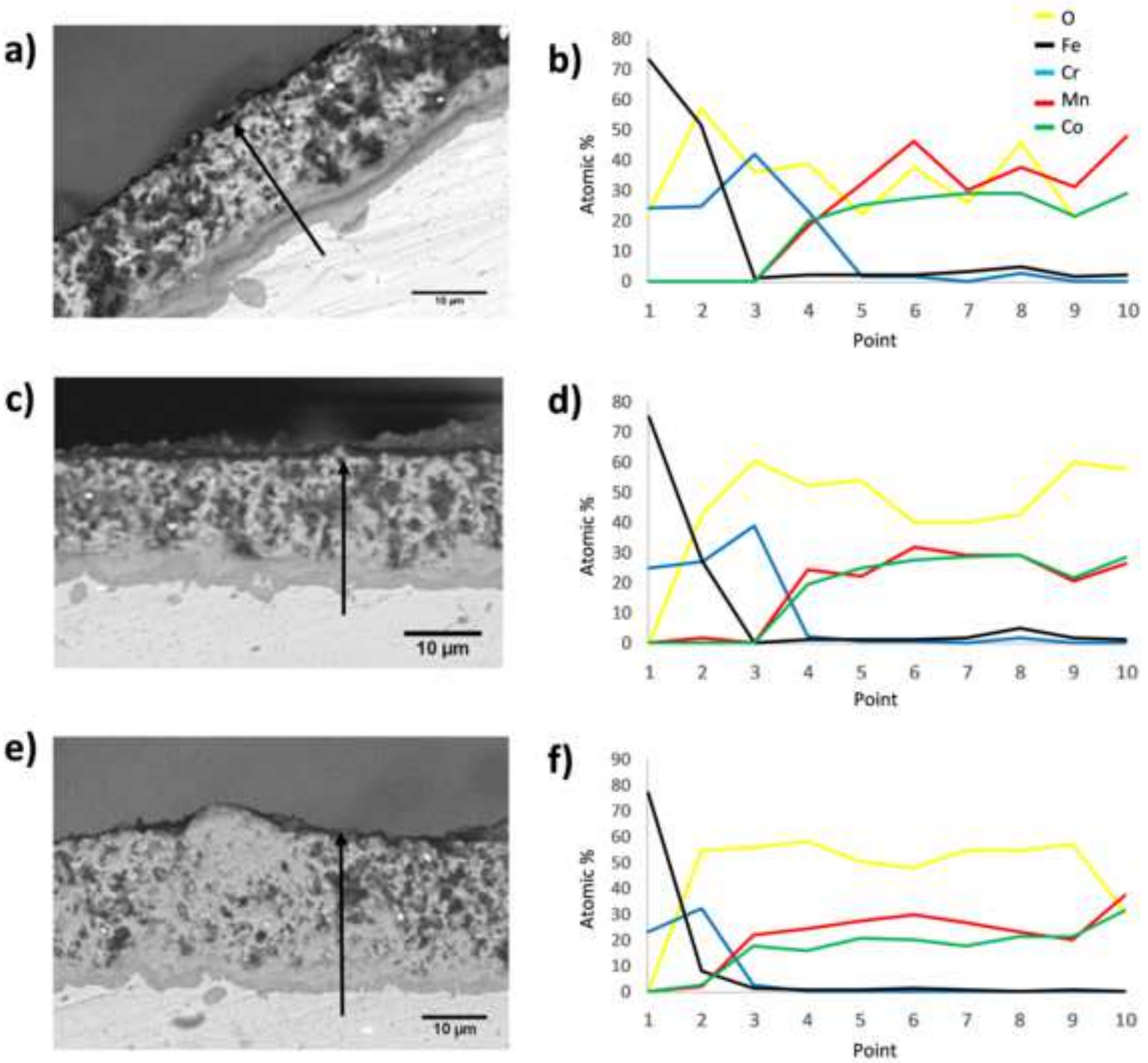

Declaration of interests

☒ The authors declare that they have no known competing financial interests or personal relationships that could have appeared to influence the work reported in this paper.

☐The authors declare the following financial interests/personal relationships which may be considered as potential competing interests: